

Co-Designing Robots by Differentiating Motion Solvers

Traiko Dinev, Carlos Mastalli, Vladimir Ivan, Steve Tonneau, Sethu Vijayakumar

Abstract— We present a modular algorithm for the computational co-design of legged robots and dynamic maneuvers. Current state-of-the-art approaches are based on random sampling or concurrent optimization. We propose a bilevel optimization approach that exploits the derivatives of the motion planning sub-problem (the inner level). Our approach allows for the use of any differentiable motion planner in the inner level, similarly to sampling methods, but also allows for an upper level that captures arbitrary design constraints and costs. Our approach can optimize the robot’s morphology and actuator parameters while considering its full dynamics, joint limits and physical constraints such as friction cones. We demonstrate these capabilities by studying jumping and trotting gaits and verify our results in a physics simulator, showing it successfully minimizes the energy used.

I. INTRODUCTION

To design a robot capable of executing dynamic motions, the engineers have to consider both the mechanical design of the robot and the motion it will enable. A traditional approach to robot design is to iterate between mechanical design and motion planning (e.g., [1]). More complex robots make this a challenging task. Designers need not only consider the mechanics but also the ability to execute the desired motion. Thus, *expert specialists* designers and many design iterations are needed.

Concurrent design (co-design [2]) aims to automate this process by optimizing both the motion and design parameters. The designer specifies a set of design parameters (e.g., morphologies or motor characteristics), constraints (e.g., collision avoidance between robot components), a high-level task (e.g., a jump) and an efficiency metric on it (e.g., energy). The algorithm then finds optimal design parameters and motions to more efficiently execute the task.

From a motion planning standpoint, we need to compute realistic motions in order to find realistic design improvements. Indeed recent advances in motion planning have resulted in complex planners that are both fast and accurate ([3]). It follows then that we should be able to leverage this to build a modular formulation of the co-design problem using state-of-the-art motion planning.

On the other hand, from a designer standpoint, we need to be able to specify arbitrary design constraints and cost functions in order to give the designer tools to fully specify all the parameters of the design.

All authors are with the Edinburgh Centre for Robotics, University of Edinburgh, UK.

This research was supported by (1) the European Commission under the Horizon 2020 project Memory of Motion (MEMMO, ID: 780684) and (2) the Engineering and Physical Sciences Research Council (EPSRC), and (3) the Alan Turing Institute.

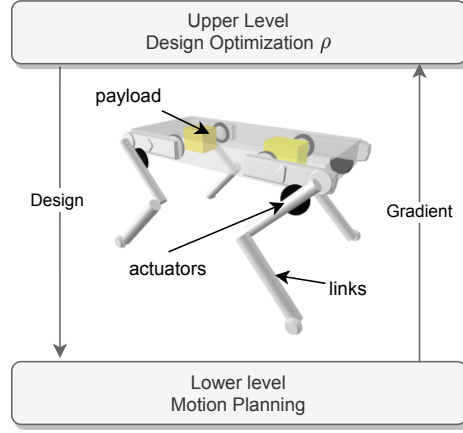


Fig. 1: Illustration of our bilevel optimization approach for robot co-design. In the upper level we use gradient information from the motion planning (lower level) to optimize the design of the robot in an iterative fashion. Please find the accompanying video at <https://youtu.be/MqG8df3wcAU>

Re-implementing motion planning in order to add additional design parameters requires considerable technical work, which is why we seek a modular framework that exploits state-of-the-art motion planners while considering design constraints. With this motivation in mind, we developed a co-design algorithm with the following scope: 1) ability to define arbitrary costs and constraints on continuous design variables, 2) treat the motion planning as a module, and 3) exploit state of the art motion planners that can compute dynamic motion for legged robots which include constraints on the motion parameters. This scope has some subtle differences from other co-design work in the literature.

A. Related Work

In the current literature, a popular approach to co-design is what we call *sampling-based co-design*. These methods are two-staged and exploit variants of Monte-Carlo sampling to find candidate robot designs. The fitness of those candidates is evaluated in a second stage through a motion planner.

The Covariance Matrix Adaptation Evolutionary Strategy (CMA-ES) [4] is a popular sampling approach used in co-design. It uses a Gaussian prior on candidate design parameters and estimates a covariance matrix needed for the following sampling steps. For instance, Wampler et al. [4] used a variant of CMA-ES to co-design various creatures in simulation, and Digumarthi et al. [5] co-designed the legs of the quadruped StarIETH to optimize its running speed. Most

recently, Chadwick et al. [6] optimized the legs of quadrupeds and bipeds over uneven terrain for different user-defined co-design metrics, and Fadini et al. [7] computed the actuator properties of a monoped using CMA-ES.

A benefit of the above approaches is that they can use any motion planner in the inner loop. However, they do not support hard constraints on the design in the upper level, requiring soft constraints and cost tuning. Moreover, in practice CMA-ES scales between quadratically and exponentially with respect to the number of design parameters (i.e., decision variables) due to the curse of dimensionality ([8], [9]). While we do not require real-time speed, more efficient algorithms would allow to prototype robots for many different tasks and environments.

On the other hand, a number of *gradient-based co-design* methods have been proposed in the literature. One approach is to optimize both motion and design parameters together, as a single nonlinear program. This approach has attracted attention for the co-design of legged robots. For instance, Mombaur [10], Buondonno et al. [11] and Spielberg et al. [12] compute the motions, lengths of the robot's limbs and/or actuator parameters in a single nonlinear program. The major drawback of this approach is the complexity of the resulting nonlinear program (e.g. [13]), and the need to modify the motion planning when including new co-design requirements, making the method non-modular.

Finally, a few recent pieces of work have proposed a new approach that uses derivative information obtained via sensitivity analysis for co-design. Ha et al. [14] proposed to extract the relationship between motion and design by using the implicit function theorem. This allowed them to optimize the design while keeping the motion on the manifold of optimal motions. In a similar fashion, Desai et al. [15] used sensitivity analysis and the adjoint method to determine the same relationship. This latter approach was used in [16] and [17] for human-in-the-loop design optimization of robots.

However, the approach of [14] optimizes one target design parameter at a time and requires user input to select that parameter during optimization. The approach used in [15]–[17] allows for optimization of all design parameters given high-level task descriptions, however one significant drawback is that the motion is computed as an unconstrained minimization, which has the potential of violating the soft physics constraints, but allows to derive the relationship between motion and design.

In this paper we demonstrate a related, but more general solution, where we directly take the derivative of the motion planner without considering the underlying optimization explicitly by treating it as a generic nonlinear function. Our approach contains an upper and a lower-level optimization for robot design and motion planning, respectively. In the lower level, we can use efficient state-of-the-art constrained motion planners – we can use any continuously differentiable motion planner. In the upper-level we formulate the co-design problem as a nonlinear program with equality and inequality constraints. We then use state-of-the-art nonlinear programming solvers and thus handle any design constraints.

Our approach bridges the gap between genetic algorithms,

which are modular and can use any motion planner, but do not natively handle design constraints and suffer from the curse of dimensionality, and gradient-based solvers, which are fast but have thus far required a modification of the motion planner or an unconstrained motion planner in case of [16] in order to derive the gradients.

B. Contributions

The main contribution of our work is a modular bilevel optimization approach for robot co-design. We identify three technical contributions:

- i. a modular co-design algorithm that differentiates a motion planner and handles arbitrary linear and nonlinear co-design constraints and any differentiable co-design cost in the upper level;
- ii. a framework and formulation for the co-design of quadrupeds for dynamic locomotion using state-of-the-art motion planning in the inner level;
- iii. a demonstration of our approach for the optimization of the morphology and actuator parameters of the quadruped SOLO for a trotting and jumping task and a verification that our locally optimal gradient-based co-design algorithm converges to the same solution as a globally optimal sampling based solver (CMA-ES).

Our approach is of practical interest, as it allows for the use of any differentiable motion planner in the inner level without any modification to the motion planning itself. A modular approach like ours can take advantage of the state-of-the-art motion planning algorithms in terms of their convergence via the efficient use of the problem structure, and their ability to solve complex problems involving full robot dynamics and contacts with the environment. We show that gradient information and a bilevel optimization is a feasible approach to co-design for real-world co-design problems.

II. CO-DESIGN PIPELINE

Our co-design pipeline has two phases (Fig. 2). In the first phase, we optimize the design and the motion of a robot using a gradient approach. In the second phase, we verify our results in a physics simulator. We begin by describing a generic bilevel formulation of the co-design problem.

A. Co-design as bilevel optimization

We begin by encoding the robot's design into a *design vector* ρ . In this paper, ρ encodes the robot's link lengths and its base shape (width, height, depth), as well as the actuator parameters – motor mass and gear ratio. We then formulate the co-design problem over the design vector ρ as a bilevel optimization problem:

$$\begin{aligned}
 & \min_{\rho, \mathbf{X}, \mathbf{U}} J_{cd}(\rho, \mathbf{X}, \mathbf{U}) && \text{(co-design metric)} \\
 & \text{s.t. } \mathbf{X}, \mathbf{U} = \text{MP}(\rho; \text{TASK}), && \text{(motion planning)} \\
 & \underline{\rho} \leq \rho \leq \bar{\rho}, && \text{(design bounds)} \\
 & \mathbf{g}(\rho) = 0, && \text{(equality design constraints)} \\
 & \mathbf{h}(\rho) \leq 0, && \text{(inequality design constraints)}
 \end{aligned} \tag{1}$$

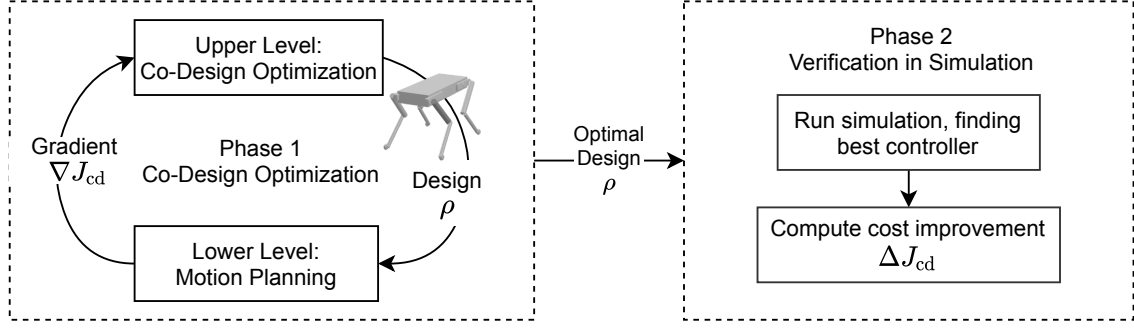


Fig. 2: A schematic of our co-design pipeline. In the first phase we optimize the robot’s design by differentiating through a motion planner (a nonlinear optimal control problem). Then, we verify the design improvements in a physics simulator using a proportional-derivative (PD) controller to track the motion plan.

where $J_{cd}(\cdot)$ is a user-specified co-design metric that evaluates the goodness of the design through the efficiency of the motion (e.g., the total energy used), $MP(\cdot)$ is the motion planning function, ρ and $\bar{\rho}$ are the lower and upper bounds of the design parameters. $g(\rho)$ and $h(\rho)$ are general equality and inequality constraints on the design vector (e.g., no collision constraints). We formulate the MP function itself as a nonlinear optimal control problem, which computes a discretized trajectory of robot states – $\mathbf{X} = \{x_0, \dots, x_N\}$ and controls $\mathbf{U} = \{u_0, \dots, u_{N-1}\}$ – for a desired task (represented by TASK) such as a trotting or jumping gait. Here N is the planning horizon, which is part of the task description.

We consider the motion planner as a general nonlinear function that maps from design parameters ρ to motions $\mathbf{m} = \{\mathbf{X}, \mathbf{U}\}$. Thus, we can write the derivative of the co-design cost as:

$$\begin{aligned} \nabla_{\rho} J_{cd} &= \frac{dJ_{cd}(\rho, \mathbf{m})}{d\rho} = \frac{\partial J_{cd}}{\partial \mathbf{m}} \frac{\partial \mathbf{m}}{\partial \rho} + \frac{\partial J_{cd}}{\partial \rho} \\ &= \frac{\partial J_{cd}}{\partial \mathbf{m}} \frac{\partial MP(\rho; \text{TASK})}{\partial \rho} + \frac{\partial J_{cd}}{\partial \rho}, \end{aligned} \quad (2)$$

where $\frac{\partial \mathbf{m}}{\partial \rho}$ is the derivative of the motion with respect to the design parameters. This derivative can be computed using sensitivity analysis of the motion planner itself. However, the resulting expression is dependent on the optimization used in the inner level and thus not a modular solution. Computing it is also cumbersome as it involves differentiating through a complex nonlinear programming program.

Instead, we can directly consider the derivative $\frac{\partial MP(\rho; \text{TASK})}{\partial \rho}$, or even more generally, directly $\nabla_{\rho} J_{cd}$. This derivative would be difficult to compute analytically, however in practice the dimension of ρ is small, compared to the dimension of the motion. For instance, in our trotting experiment, $\dim(\rho) = 17$, while $\dim(\mathbf{m}) = 9163$. Hence we can obtain $\nabla_{\rho} J_{cd}$ directly through a numerical differentiation procedure that runs in parallel, i.e., we compute the derivative for each component of the design vector using multiprocessing. Using a one-sided finite difference approach, this requires a total of $\dim(\rho) - 1$ calls to the motion planner. For each component of ρ , we

have:

$$\nabla_{\rho_i} J_{cd} \approx \frac{J_{cd}(\rho_i^+, MP(\rho_i^+; \text{TASK})) - J_{cd}(\rho, MP(\rho; \text{TASK}))}{\epsilon} \quad (3)$$

where ρ_i^+ is the design vector with ϵ added to its i^{th} element.

Using the derivative $\nabla_{\rho} J_{cd}$, we can then optimize the design with gradient-based optimization.

This approach directly considers the motion as a function of the motion planner and does not assume a particular form of motion planning. Thus it allows us to use the full rigid body dynamics, friction cone constraints, control and state bounds in a nonlinear optimal control formulation (motion planner).

So far we have described our bilevel formulation of the co-design problem. We next describe our formulation of the co-design problem for quadrupeds, followed by the motion planning level.

B. Co-design: outer level

We focus our work on improving the design of the 12 Degrees of Freedom (DoFs) SOLO robot [18]. Particularly, we are interested in quadrupedal locomotion gaits such as trotting and jumping. To plan for these gaits, the motion planner takes as parameters the following:

- The task, which is the desired gait, consisting of the contact sequence and timings
- The initial joint configuration q_0
- The robot’s joint limits

Each of these are computed in the upper level from the design vector ρ and updated each time the optimizer calls the motion planner to compute the optimal trajectory. We compute the initial state of the robot q_0 using inverse kinematics so that the angle at the knee joint of the shortest leg is 45° . We then run forward kinematics to set the foot positions, gait sequence and timings based on the task. We used the library PINOCCHIO [19] for computing the robot’s kinematics and dynamics. We also set the lower and upper control bounds (\underline{u}, \bar{u}), and finally compute the optimal motion. We present an overview of our co-design optimization algorithm in Algorithm 1. In the upper level, we use the solver KNITRO [20] with an interior-point/direct algorithm,

Algorithm 1 Co-design optimization

```

1: procedure MP( $\rho$ ; TASK)
2:   Compute initial state  $q_0$  using inverse kinematics
3:   Set control bounds  $\underline{u}, \bar{u}$  based on actuator parameters
4:   Run forward kinematics on  $q_0$  and set foot positions
5:   Set gait sequence and timings based on TASK
6:   Compute  $m$ , the optimal motion
7:   return  $m$ 
8: end procedure
9: procedure CODESIGN
10:  Start at a design  $\rho = \rho_0$ 
11:  while  $J_{cd}(\rho, \text{MP}(\rho; \text{TASK}))$  decreasing do
12:    Compute  $\nabla_\rho J_{cd}$  via finite differences in parallel
13:    Update  $\rho$  using one step of the NLP solver
14:    Save the resulting motion to  $m$  and cost  $J_{cd}$ 
15:  end while
16:  return  $(\rho, J_{cd})$  – optimal design and its cost value
17: end procedure

```

providing the derivatives of the motion planner using the parallel scheme described.

C. Motion planning: inner level

The lower level of our co-design bilevel optimization algorithm computes the motion trajectory $\{X, U\}$ given a task and design ρ . We formulate this inner optimization as a hybrid nonlinear optimal control problem with fixed contact sequence and timings (Equation (4)):

$$\begin{aligned}
& \arg \min_{X, U} \sum_{k=0}^{N-1} \|\mathbf{q}_k \ominus \mathbf{q}_{\text{ref}}\|_Q^2 + \|\mathbf{v}_k\|_N^2 + \|\mathbf{u}_k\|_R^2 + \|\boldsymbol{\lambda}_k\|_K \\
& \text{s.t.} \\
& \text{for each contact phase: } p \in \mathcal{P} = \{1, 2, \dots, N_p\} \\
& \quad \text{if } \underline{\Delta t}_p \leq k \leq \bar{\Delta t}_p: \\
& \quad \quad \mathbf{q}_{k+1} = \mathbf{q}_k \oplus \int_{t_k}^{t_k + \Delta t_k} \mathbf{v}_k \, dt, \quad (\text{integrator}) \\
& \quad \quad \mathbf{v}_{k+1} = \mathbf{v}_k + \int_{t_k}^{t_k + \Delta t_k} \dot{\mathbf{v}}_k \, dt, \\
& \quad \quad (\dot{\mathbf{v}}_k, \boldsymbol{\lambda}_k) = \mathbf{f}_p(\mathbf{q}_k, \mathbf{v}_k, \mathbf{u}_k), \quad (\text{contact dyn.}) \\
& \quad \text{else:} \\
& \quad \quad \mathbf{q}_{k+1} = \mathbf{q}_k, \\
& \quad \quad (\mathbf{v}_{k+1}, \boldsymbol{\lambda}_k) = \Delta_p(\mathbf{q}_k, \mathbf{v}_k), \quad (\text{impulse dyn.}) \\
& \quad \quad \mathbf{g}(\mathbf{q}_k, \mathbf{v}_k, \mathbf{u}_k) = \mathbf{0}, \quad (\text{equality}) \\
& \quad \quad \mathbf{h}(\mathbf{q}_k, \mathbf{v}_k, \mathbf{u}_k) \leq \mathbf{0}, \quad (\text{inequality}) \\
& \quad \quad \underline{x} \leq \mathbf{x}_k \leq \bar{x}, \quad (\text{state bounds}) \\
& \quad \quad \underline{u} \leq \mathbf{u}_k \leq \bar{u}. \quad (\text{control bounds})
\end{aligned} \tag{4}$$

The state $(\mathbf{q}, \mathbf{v}) \in X$ lies in a differential manifold formed by the configuration $\mathbf{q} \in \text{SE}(3) \times \mathbb{R}^{n_j}$ and its tangent vector $\mathbf{v} \in \mathbb{R}^{n_x}$ (with n_x and n_j as the dimension of the state manifold and number of joints, respectively). The control

$\mathbf{u} \in \mathbb{R}^{n_j}$ is the vector of input torques, $\boldsymbol{\lambda}_k$ is the vector of contact forces, \ominus and \oplus are the *difference* and *integration* operators of the state manifold, respectively. Then \mathbf{q}_{ref} is the reference robot posture, and $\mathbf{f}_p(\cdot)$ represents the contact dynamics under the phase p . To account for effects of discrete contact changes, $\Delta_p(\cdot)$ is used to define an autonomous system that describes the contact-gain transition ([21]). Q , N , R and K are positive-define weighting matrices, (\underline{x}, \bar{x}) and (\underline{u}, \bar{u}) are the lower and upper bounds of the system state and control. $\underline{\Delta t}_p$ and $\bar{\Delta t}_p$ defines the timings of the contact phase p . We compute the hybrid dynamics and its derivatives as described in [3].

During contact phases, we only include the friction-cone constraint via a linearized cone $(A\boldsymbol{\lambda}_{C(k)} \leq \mathbf{r})$, where (A, \mathbf{r}) are computed from a predefined number of edges, and minimum and maximum normal contact forces, respectively. $C(k)$ describes the set of active contacts. In contrast, during the swing phases, we also include contact-placement constraints $(\log(\mathbf{p}_{G(k)}^{-1} \circ M_{P_{G(k)}}) = \mathbf{0})$, where $\log(\cdot)$ describes the log operator used in Lie algebra, $\mathbf{p}_{G(k)}$ and $M_{P_{G(k)}}$ are the reference and current placements of the set of swing contacts $G(k)$.

We solve the motion planning problem formulated in Eq. (4) with Feasibility-Driven Control-limited DDP (Box-FDDP) [22], which is a variant of the Differential Dynamic Programming (DDP) algorithm. Box-FDDP uses direct-indirect hybridization and enforces hard-constraints for the control limits. We employ a soft quadratic barrier to enforce inequality, equality and state constraints defined in Eq. (4). We implemented the algorithm using the open-source library CROCODDYL [3].

D. Verification in simulation

The second phase of our co-design pipeline validates the design improvements in the PYBULLET physics simulator. ([23]). To do so, we execute the motion plan for both the nominal and the optimized designs, and record the percentage improvement in costs ΔJ_{cd} (similar to [24]). We use a proportional-derivative (PD) controller with feed-forward torque to track the planned motion:

$$\mathbf{u} = \mathbf{u}^* + \mathbf{K}_p(\mathbf{q}_j^* - \mathbf{q}_j) + \mathbf{K}_d(\mathbf{v}_j^* - \mathbf{v}_j),$$

where \mathbf{u}^* , \mathbf{q}_j^* and \mathbf{v}^* are the reference feed-forward command, joint positions and velocities computed in Eq. (4), respectively. \mathbf{K}_p and \mathbf{K}_d are the PD gains. We tune these gains through a grid search procedure. We run the simulator on a 20×20 grid for $\mathbf{K}_p \in [1, 20]$ and $\mathbf{K}_d \in [0.1, \mathbf{K}_d/2]$. Then, we pick the gains that lead to the smallest tracking error for both designs. This procedure allows us to fairly compare and account for different robot dimensions and weights, as larger robots require higher gains and vice-versa.

Next, we provide more details about the co-design parameters and cost metrics used in this work.

III. CO-DESIGN FORMULATION – ROBOT MODEL, COST FUNCTION AND CONSTRAINTS

Our design vector ρ consists of the lengths of the lower- and upper-leg limbs, the x-, and z-attachment position of the

legs, the trunk shape: width, height and depth. Additionally, we model the position of the two electronics boxes in the base of the robot along the x and z directions. We thus implicitly constrain the design to be symmetrical along the direction of motion (the y-direction).

Next, we use an actuator model and optimize both the gear ratio and motor mass, which are the same for all motors, for simplicity. All these properties are included in the robot model to compute masses and inertias of the relevant links. For the limbs, we scale the volume linearly with the length of the leg as a simple proxy measure for structural integrity.

A. Actuator Model and Cost Function

Following [7] and [25] we model the mass of the motor m_m and parameterize the control limits \underline{u} and \bar{u} using an exponential regression based on m_m . We used the same values as [7], namely:

$$\bar{u} = -\underline{u} = 5.48 m_m^{0.97}. \quad (5)$$

Following [7], the dynamics of the system in the motion planning phase are frictionless and the actuator model is present in the co-design cost function. Given applied controls \mathbf{u} at the robot's joints, the total torque at the motor (τ_t) is:

$$\tau_t = \frac{\mathbf{u}}{n} + \tau_f, \quad (6)$$

where n is the gear ratio and τ_f – the friction torque. The friction torque itself models the combined Coulomb and viscous friction at the transmission, which the motor needs to overcome. Thus:

$$\tau_f = \tau_\mu \operatorname{sign}(\omega_m) + b \omega_m, \quad (7)$$

where τ_μ is the Coulomb friction parameter, b – the viscous friction parameter and ω_m is the motor angular speed, which is n times the joint angular speed.

We then consider three power losses – mechanical power, Joule effect from the motor winding resistance, and friction losses from the transmission:

$$P_{\text{mech}} = \tau_f \omega_m, \quad P_{\text{joule}} = \frac{1}{K_m} \tau_f^2, \quad P_{\text{fric}} = \tau_f \omega_m, \quad (8)$$

where $K_m = 0.15 m_m^{1.39}$ is the speed-torque gradient of the motor, again computed using an exponential regression on the motor mass.

Unlike in [7], we cannot ignore the mechanical power, as the foot start and end positions are dependent on the robot body structure and the total energy is not conserved between designs (and thus not constant). We thus follow [25] and compute the integral of the above terms ignoring power regenerative effects, summed over each of the motors:

$$J_{\text{cd}} = \int_{t_0}^{t_N} \sum_{\text{motor}} P_{\text{elec}} + \max(P_{\text{fric}}, 0) \, dt, \quad (9)$$

where $P_{\text{elec}} = \max(P_{\text{mech}} + P_{\text{joule}}, 0)$ is the positive electrical work (as defined in [25]). The friction power is separate, as it is due to the transmission. We integrate over the planning horizon and sum the non-negative power of each of the 12 SOLO motors. Thus $J_{\text{cd}}(\cdot)$ is the integral of these power terms, corresponding to the energy used during the motion.

B. Constraints

We then specify constraints on the design vector ρ . Firstly, we add a volumetric collision constraint on the electronics boxes, the Inertial Measurement Unit (IMU) box and the motherboard (MB) box:

$$(x_{\text{mb}} - z_{\text{imu}})^2 + (x_{\text{mb}} - z_{\text{imu}})^2 \leq (r_{\text{mb}} + r_{\text{imu}})^2, \quad (10)$$

where $x_{\text{mb}}, z_{\text{mb}}, x_{\text{imu}}, z_{\text{imu}}$ are the coordinates of the two boxes and $r_{\text{mb}} = 0.0361\text{m}$, $r_{\text{imu}} = 0.0282\text{m}$ are the radii of the smallest circumscribed sphere around them.

Finally, we specify linear constraints on the positions of the two electronics boxes and the positions of the legs so that they are within the base of the robot:

$$\begin{aligned} -\frac{w_b}{2} \leq x_{\text{imu}} \leq \frac{w_b}{2}, \quad -\frac{w_b}{2} \leq x_{\text{mb}} \leq \frac{w_b}{2}, \quad -\frac{d_b}{2} \leq z_{\text{imu}} \leq \frac{d_b}{2}, \\ -\frac{d_b}{2} \leq z_{\text{imu}} \leq \frac{d_b}{2}, \quad -\frac{w_b}{2} \leq x_{\text{fr}} \leq \frac{w_b}{2}, \quad -\frac{w_b}{2} \leq x_{\text{hr}} \leq \frac{w_b}{2}, \\ -\frac{d_b}{2} \leq z_{\text{fr}} \leq \frac{d_b}{2}, \quad -\frac{d_b}{2} \leq z_{\text{hr}} \leq \frac{d_b}{2} \end{aligned} \quad (11)$$

where w_b and d_b are the width and depth of the base and $x_{\text{fr}}, z_{\text{fr}}$ and $x_{\text{hr}}, z_{\text{hr}}$ are the x- and z-coordinates of the front and hind shoulders. Note these inequalities constraints are defined in the upper level optimization.

C. Task Description

For trotting, the high-level motion task is to take two steps forward, each of 0.05m, with a fixed step height of 0.05m. We allocated 22 and 37 knots¹ for the swing and double support phases of the motion, respectively, and used a symplectic Euler integrator with time-step of 10ms.

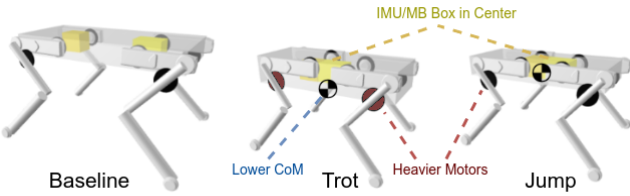
For jumping, the high-level motion task is to jump forward 0.1m with a step height of 0.15m. We used the same integrator and time-step as in the trotting case. We defined 20 knots for the flight phase and 40 knots for the take-off and landing phases.

D. Results

The resulting robot designs and cost improvements are in Figures 3a and 3b, respectively. For both trotting and jumping, We plotted the positive electrical work at the motor as P_{elec} versus the friction contribution from the transmission as P_{fric} . The algorithm chooses to minimize the electro-mechanical losses while increasing the friction losses. This is similar to [7], as we find that small motors are much more energy inefficient since the reciprocal of the speed-torque gradient exponentially decreases ($K_m = 0.15 m_m^{1.39}$), increasing the Joule losses.

For trotting specifically, the friction losses are smaller, as trotting is a more static motion with smaller motor velocities, and friction is velocity-dependent. Thus the dominating cost is the electro-mechanical energy. This allows for a heavier robot with bigger motors than the optimal design for a jumping task – the optimal motor mass is $m_m = 0.179\text{kg}$. and gear ratio – $N = 16.062$ with a total robot weight of 3.805kg..

¹Knots are points in time for the discretization of the optimal control problem.



(a) Resulting robot designs for trotting and jumping.

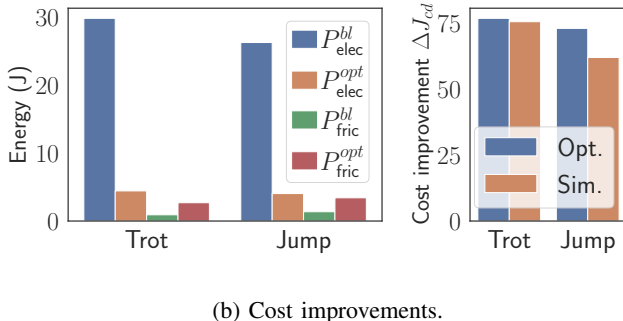


Fig. 3: Robot designs and cost improvements on the trotting and jumping tasks. The costs are broken down for electric and friction contributions. We show the optimization and simulation percentage improvement on the bottom right.

The initial motor mass and gear ratio for the SOLO robot are $m_m = 0.053\text{kg}$. and $N = 9$ and the robot weighs 2.421kg . With a higher gear ratio the optimizer reduced the electro-mechanical energy further. Furthermore, we see a increase in base depth, which allows for the upper legs to be attached higher to the base of the robot. This allows for a lower center of mass, which can increase stability.

For jumping, however, a heavy robot is not optimal, as the entire mass of the robot needs to be moved. Thus the optimizer found $m_m = 0.168$ and $N = 17.325$ with a total mass of 3.592kg . The robot is heavier than the baseline, however the legs and the base are smaller. Compared to the optimal trotting design, the motors are lighter, but the gear ratio for both designs is similar. For both optimal designs, notably the boxes are optimally in the middle of the robot.

Finally, for both optimal designs, we also observed that the cost improvements remain in simulation within 10% of the ones found during optimization.

E. Optimality and Scalability

We compared our gradient-based co-design approach to the CMA-ES genetic algorithm on the trotting task in order to check convergence properties and optimality. We used the open-source CMA-ES library PYCMA library [26]. In order to evaluate scalability, we varied the dimensions of the co-design vector by including subsets of the decision variables, namely:

- 1) $\dim(\rho) = 4$ – leg lengths (front and back)
- 2) $\dim(\rho) = 6$ – same as 4, and motor mass and gear ratio
- 3) $\dim(\rho) = 9$ – same as 6, and base shape
- 4) $\dim(\rho) = 13$ – same as 9, and electronics boxes

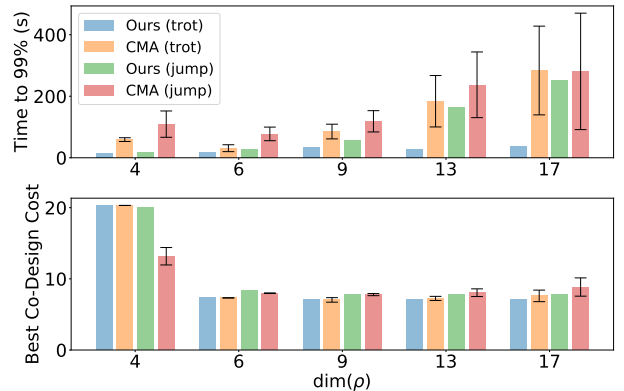


Fig. 4: Scalability results for different problem dimensions.

5) $\dim(\rho) = 17$ – full model

For CMA-ES we specified a quadratic soft penalty for all constraints. We ran CMA-ES with population sizes $N = [10, 20, 50]$ and selected $N = 50$, which achieved the same or lower costs than our approach on all problems. We then plot the mean cost and standard deviation as well as mean time to 99% convergence and standard deviation over 20 runs at $N = 50$ in Figure 4. On the trotting task our approach has better scalability than CMA-ES, which is expected given the convergence properties of CMA-ES. On the jumping task convergence is slower for both with CMA-ES having a large deviation in convergence time for larger problems. Of interest is that we are able to achieve similar best co-design costs as CMA-ES across problem dimensions for the given co-design problems. This could indicate that our local gradient-based bilevel approach can achieve globally optimal solutions in practice, for problems like the ones studied here.

IV. DISCUSSION

In this paper we proposed a modular co-design algorithm and pipeline for dynamic quadruped locomotion. Our approach is based on bilevel optimization and exploits the derivatives of a hybrid nonlinear optimal control problem (inner problem that describes the motion planner).

In our experiments we noted that a coupling between the outer and inner level costs is beneficial. In this work we have a weak coupling, where the inner layer has a regularization on the square of the torques and the outer layer has the Joule effect cost, also on the square of the torques.

Future work lies in using analytical derivatives instead of using finite differences, which introduce numerical errors when computing the derivative of the motion planner. Furthermore, our approach can use any differentiable motion planner and there are interesting opportunities in using different motion planners and formulations (for instance different contact models and constraints) which can enable co-design in more complex domains, for instance with sliding or slipping contacts. Additionally, of interest is handling more complex state constraints that come from the environment, for instance for footstep planning – determining the contact locations and timings of footsteps.

REFERENCES

[1] C. Semini, N. G. Tsagarakis, E. Guglielmino, M. Focchi, F. Cannella, and D. G. Caldwell, "Design of HyQ - a hydraulically and electrically actuated quadruped robot," *Journal of Systems and Control Engineering*, vol. 225, 2011.

[2] Q. Li, W. Zhang, and L. Chen, "Design for control-a concurrent engineering approach for mechatronic systems design," vol. 6, 2001.

[3] C. Mastalli, R. Budhiraja, W. Merkt, G. Saurel, B. Hammoud, M. Naveau, J. Carpentier, L. Righetti, S. Vijayakumar, and N. Mansard, "Crocoddyl: An Efficient and Versatile Framework for Multi-Contact Optimal Control," in *IEEE ICRA*, 2020.

[4] K. Wampler and Z. Popović, "Optimal gait and form for animal locomotion," *ACM Transactions on Graphics*, vol. 28, 2009.

[5] K. M. Digumarti, C. Gehring, S. Coros, J. Hwangbo, and R. Siegwart, "Concurrent optimization of mechanical design and locomotion control of a legged robot," in *Mobile Service Robotics*. World Scientific, 2014.

[6] M. Chadwick, H. Kolvenbach, F. Dubois, H. F. Lau, and M. Hutter, "Vitruvio: An Open-Source Leg Design Optimization Toolbox for Walking Robots," *IEEE Robot. Automat. Lett. (RA-L)*, vol. 5, 2020.

[7] G. Fadini, T. Flayols, A. del Prete, N. Mansard, and P. Souères, "Computational design of energy-efficient legged robots: Optimizing for size and actuators," in *ICRA2021*, 2020.

[8] M. N. Omidvar and X. Li, "A comparative study of cma-es on large scale global optimisation," in *Australasian Joint Conference on Artificial Intelligence*. Springer, 2010, pp. 303–312.

[9] N. Hansen, "Benchmarking a bi-population cma-es on the bbo-b-2009 function testbed," in *Proceedings of the 11th Annual Conference Companion on Genetic and Evolutionary Computation Conference: Late Breaking Papers*, 2009, pp. 2389–2396.

[10] K. Mombaur, "Using optimization to create self-stable human-like running," *Robotica*, vol. 27, 2009.

[11] G. Buondonno, J. Carpentier, G. Saurel, N. Mansard, A. De Luca, and J.-P. Laumond, "Actuator design of compliant walkers via optimal control," in *IEEE/RSJ IROS*, 2017.

[12] A. Spielberg, B. Araki, C. Sung, R. Tedrake, and D. Rus, "Functional co-optimization of articulated robots," in *IEEE ICRA*, 2017.

[13] W. Sun, G. Tang, and K. Hauser, "Fast uav trajectory optimization using bilevel optimization with analytical gradients," in *2020 American Control Conference (ACC)*. IEEE, 2020, pp. 82–87.

[14] S. Ha, S. Coros, A. Alspach, J. Kim, and K. Yamane, "Computational co-optimization of design parameters and motion trajectories for robotic systems," *The International Journal of Robotics Research*, vol. 37, 2018.

[15] R. Desai, B. Li, Y. Yuan, and S. Coros, "Interactive Co-Design of Form and Function for Legged Robots using the Adjoint Method," *arXiv:1801.00385 [cs]*, Apr. 2018, arXiv: 1801.00385. [Online]. Available: <http://arxiv.org/abs/1801.00385>

[16] M. Geilinger, R. Poranne, R. Desai, B. Thomaszewski, and S. Coros, "Skaterbots: optimization-based design and motion synthesis for robotic creatures with legs and wheels," *ACM Transactions on Graphics*, vol. 37, 2018.

[17] M. Geilinger, S. Winberg, and S. Coros, "A Computational Framework for Designing Skilled Legged-Wheeled Robots," *IEEE Robot. Automat. Lett. (RA-L)*, vol. 5, 2020.

[18] F. Grimminger, A. Meduri, M. Khadiv, J. Viereck, M. Wüthrich, M. Naveau, V. Berenz, S. Heim, F. Widmaier, T. Flayols, J. Fiene, A. Badri-Spröwitz, and L. Righetti, "An Open Torque-Controlled Modular Robot Architecture for Legged Locomotion Research," *IEEE Robot. Automat. Lett. (RA-L)*, vol. 5, 2020.

[19] J. Carpentier, G. Saurel, G. Buondonno, J. Mirabel, F. Lamiriaux, O. Stasse, and N. Mansard, "The pinocchio c++ library: A fast and flexible implementation of rigid body dynamics algorithms and their analytical derivatives," in *2019 IEEE/SICE International Symposium on System Integration (SII)*. IEEE, 2019, pp. 614–619.

[20] R. H. Byrd, J. Nocedal, and R. A. Waltz, "K nitro: An integrated package for nonlinear optimization," in *Large-scale nonlinear optimization*. Springer, 2006, pp. 35–59.

[21] R. Featherstone, *Rigid Body Dynamics Algorithms*. Berlin, Heidelberg: Springer-Verlag, 2007.

[22] C. Mastalli, W. Merkt, J. Marti-Saumell, H. Ferrolho, J. Sola, N. Mansard, and S. Vijayakumar, "A Direct-Indirect Hybridization Approach to Control-Limited DDP," 2021.

[23] E. Coumans and Y. Bai, "Pybullet, a python module for physics simulation for games, robotics and machine learning," *GitHub repository*, 2016.

[24] L. Pecyna, A. Cangelosi, and A. Di Nuovo, "A Deep Neural Network for Finger Counting and Numerosity Estimation," in *IEEE Symposium Series on Computational Intelligence (SSCI)*, 2019.

[25] Y. Yesilevskiy, Z. Gan, and C. David Remy, "Energy-optimal hopping in parallel and series elastic one-dimensional monopeds," *Journal of Mechanisms and Robotics*, vol. 10, no. 3, p. 031008, 2018.

[26] N. Hansen, Y. Akimoto, and P. Baudis, "CMA-ES/pycma on Github," Zenodo, DOI:10.5281/zenodo.2559634, 2019.